Probing Dynamics of an Electron-Spin Ensemble via a Superconducting Resonator

V. Ranjan,[1] G. de Lange,[1] R. Schutjens,[1] T. Debelhoir,[2] J. P. Groen,[1] D. Szombati,[1]
D. J. Thoen,[1] T. M. Klapwijk,[1] R. Hanson,[1] and L. DiCarlo[1]

[1]*Kavli Institute of Nanoscience, Delft University of Technology, P.O. Box 5046, 2600 GA Delft, The Netherlands*
[2]*ICFP, Département de Physique de l'ENS, 24 rue Lhomond, 75005 Paris, France*

(Received 27 August 2012; published 8 February 2013)

We study spin relaxation and diffusion in an electron-spin ensemble of nitrogen impurities in diamond at low temperature (0.25–1.2 K) and polarizing magnetic field (80–300 mT). Measurements exploit field-controlled coupling of the ensemble to two modes of a transmission-line resonator. The observed temperature-independent spin relaxation time indicates that spin outdiffusion across the mode volume dominates over spin-lattice relaxation. Depolarization of one hyperfine-split subensemble by pumping of another indicates fast cross relaxation, with implications for the use of subensembles as independent quantum memories.

DOI: 10.1103/PhysRevLett.110.067004 PACS numbers: 85.25.−j, 03.67.Lx, 42.50.Pq, 76.30.−v

The study of spin ensembles coupled to superconducting integrated circuits is of both technological and fundamental interest. An eventual quantum computer may involve a hybrid architecture [1–4] combining superconducting qubits for processing of information, solid-state spins for storage, and superconducting resonators for interconversion. Additionally, superconducting resonators allow the study of spin ensembles at low temperatures with ultralow excitation powers and high spectral resolution [5,6]. While one spin couples to one microwave photon with strength $g/2\pi \sim 10$ Hz, an ensemble of N spins collectively couples with $g_{\mathrm{ens}} = g\sqrt{N}$ [7,8], reaching the strong-coupling regime $g_{\mathrm{ens}} > \kappa, \gamma$ at $N \gtrsim 10^{12}$ [8–10], where κ and γ are the circuit damping and spin dephasing rates, respectively.

Among the solid-state spin ensembles under consideration, nitrogen defects in diamond ($P1$ centers) [11] are excellent candidates for quantum information processing. Diamond samples can be synthesized with $P1$ centers as only paramagnetic impurities. Additionally, samples with spin densities ranging from highly dense (> 200 ppm) to very dilute (< 5 ppb) are commercially available, allowing the tailoring of spin linewidth ($\gamma \propto N$ [12]) and collective strength ($g_{\mathrm{ens}} \propto \sqrt{N}$). In contrast to nitrogen-vacancy centers in diamond [13] and rare-earth ions in Y_2SiO_5 [14,15], $P1$ centers are optically inactive, making a coupled microwave resonator an ideal probe for their study. However, the magnetic fields $\gtrsim 100$ mT needed to polarize the ensemble at the few-GHz transition frequencies of circuits [16] must not compromise superconductivity. The freezing of spin dynamics in a high-purity $P1$ ensemble by the field would allow quenching spin decoherence [17]. Further enhancing the quenching with dynamical decoupling techniques [18] will make $P1$ ensembles useful quantum memories in hybrid architectures.

In this Letter, we investigate the dynamics of a semi-polarized $P1$ electron-spin ensemble using magnetic-field controlled interaction with two modes of a coplanar-waveguide NbTiN resonator [19]. Three hyperfine-split spin subensembles are clearly resolved in the 0.25–1.2 K temperature range, with collective coupling strength extrapolating to $g_{\mathrm{ens}}/2\pi = 23$ MHz at full polarization. The coupling to multiple modes allows distinguishing the contributions of dipolar broadening and magnetic-field inhomogeneity to the spin linewidth. Furthermore, we observe temperature-independent spin repolarization, and conclude that polarization dynamics are dominated by spin diffusion [20] rather than spin-lattice relaxation [21]. Finally, cross relaxation between hyperfine-split subensembles is studied for the first time in a hybrid architecture. We find clear evidence that cross relaxation is fast compared to the repolarization, which may impact the use of $P1$ subensembles as independent quantum memories.

Our hybrid system, shown schematically in Fig. 1, consists of four resonators capacitively coupled to a common feed line and a type-Ib diamond sample placed above one of them. The electron-spin ensemble consists of unpaired electrons (spin-1/2) at substitutional nitrogen impurities [Fig. 1(a)]. Each electron spin exhibits strong anisotropic hyperfine interaction with the host nucleus (spin-1). The Hamiltonian for one defect is given by $H_{\mathrm{N}} = -m_0\vec{B}\cdot\vec{S} + h\vec{S}\cdot A\cdot\vec{I}$, with $\vec{S}$ and $\vec{I}$ the spin operators for the electron and nitrogen nucleus, respectively, $m_0/h = 28.0$ MHz/mT, h Planck's constant, and $A = \mathrm{diag}(81.33, 81.33, 114.03)$ MHz the hyperfine interaction tensor [22] [third (first, second) index parallel (normal) to the Jahn-Teller axis]. Low-energy terms only involving $\vec{I}$ have been left out. We tune the electron-spin transitions with a magnetic field ($B_{\|}$) applied along the diamond [100] direction. Because all N-C bonds have ⟨111⟩ orientation and make the same angle with $B_{\|}$, the hyperfine interaction is the same for all impurities, creating three hyperfine-split electron-spin transitions [11].

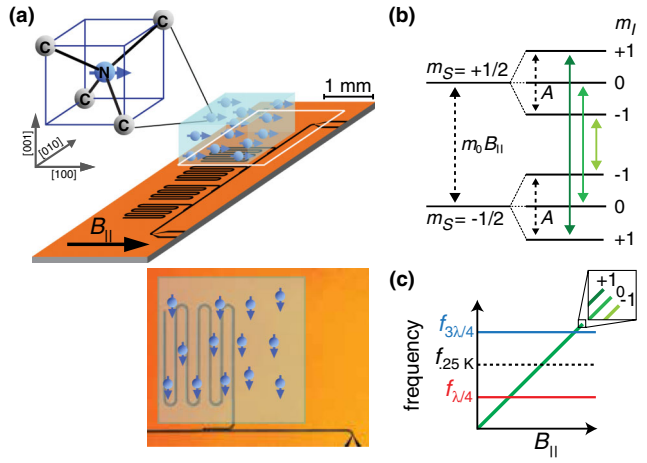

FIG. 1 (color online). (a) Schematic of the hybrid resonator-spin system. A single-crystal diamond piece (1.7 mm × 1.7 mm × 1.1 mm, type-Ib Sumicrystal, ~200 ppm N content) is placed on top of one of four coplanar-waveguide resonators capacitively coupled to a common feed line. The resonators (with 10 μm central conductor and 1.5 μm gap widths) are patterned on a NbTiN film (70 nm thick, critical temperature $T_c = 12.5$ K) on sapphire (C-plane, 430 μm thick). An external magnetic field $B_{||}$ is applied parallel to the film, along the diamond [100] direction. (b) Hyperfine interaction $A \approx 94$ MHz with the N host nuclear spin splits each electron-spin level into a triplet. Only electron-spin transitions that preserve nuclear spin (solid arrows) are allowed. (c) $B_{||}$ tunes the electron-spin energy levels through resonance with the $\lambda/4$ or $3\lambda/4$ modes of the resonator. The dashed line represents the thermal energy $k_BT/h \approx 5$ GHz at $T = 0.25$ K.

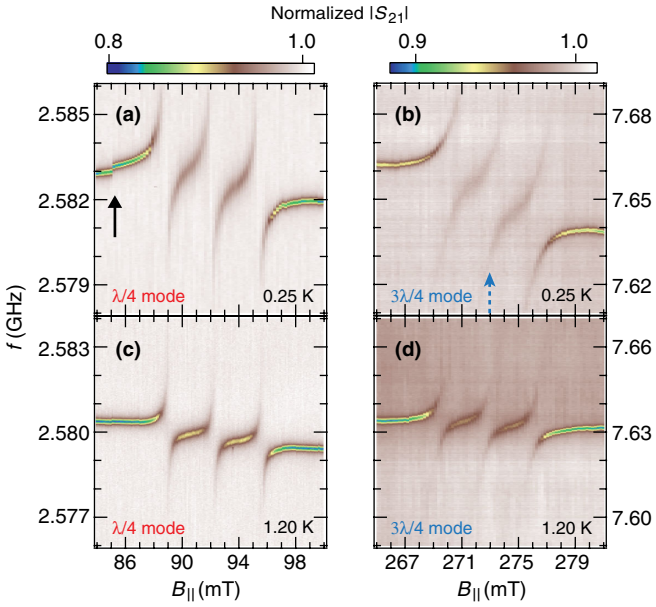

FIG. 2 (color online). Transmission spectroscopy. Image plots of normalized feed line transmission as a function of $B_{||}$ and frequency near the $\lambda/4$ and $3\lambda/4$ mode resonances at $T = 0.25$ K (a), (b) and 1.2 K (c), (d). Each plot reveals three avoided crossings, corresponding to allowed hyperfine-split electron-spin transitions. Note that the frequency span in (b), (d) is 10 times larger than in (a), (c). The arrow in (a) points to a flux jump shifting the resonator frequency. All other image plots shown are corrected for these rare events.

Measurements [23] of the feed line transmission $|S_{21}|(f, B_{||})$ near the fundamental ($\lambda/4$) and the second-harmonic ($3\lambda/4$) modes at $T = 0.25$ and 1.2 K clearly show three avoided crossings [10], as expected for coherent coupling [24] (Fig. 2). The coupling strength of each hyperfine transition to the $3\lambda/4$ mode is evidently stronger than to the $\lambda/4$ mode and decreases for both modes with increasing temperature. Note that the frequency span in Figs. 2(b) and 2(d) is 10 times larger than in Figs. 2(a) and 2(c). The hybridized dips observed when spin subensembles are resonant with the $3\lambda/4$ mode [Fig. 3(a)] support strong coupling ($2g_{\rm ens} > \gamma, \kappa$). The absence of double dips on resonance with the $\lambda/4$ mode indicates $2g_{\rm ens} < \gamma$.

We extract $g_{\rm ens}$ using the model presented in Ref. [10], treating the spin subensembles as separate harmonic oscillators coupled to the resonator, but not to each other:

$$S_{21}(\omega) = 1 + \frac{\kappa_e/2}{i\Delta_c - (\kappa_i + \kappa_e)/2 + \sum_n \frac{g_{\rm ens}^2}{i(\Delta_n) - \gamma/2}}. \quad (1)$$

Here, $\Delta_c = \omega - \omega_c$ is the frequency detuning between the probe and bare resonator mode, κ_i and κ_e are the resonator intrinsic and extrinsic dissipation rates, $\Delta_n = \omega - \omega_{m_I=n}$ is the probe detuning from the $m_I = n$ hyperfine transition,

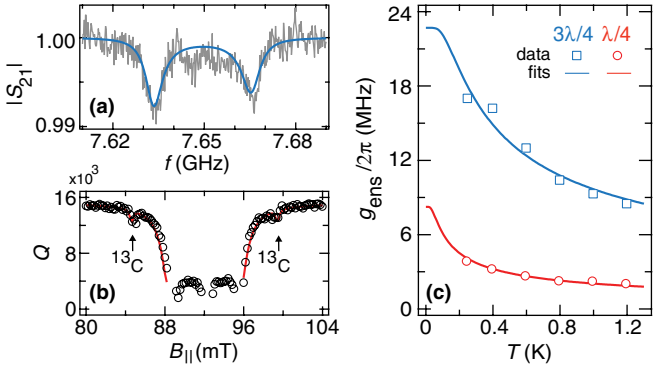

FIG. 3 (color online). Determination of the collective coupling strength $g_{\rm ens}$. (a) A vertical cut of Fig. 2(b) at $B_{||} = 272.8$ mT (dashed arrow) shows Rabi-split transmission dips. The best-fit to Eq. (1) gives $g_{\rm ens}/2\pi = 17.0$ MHz. (b) Measured loaded quality factor of the $\lambda/4$ mode as a function of $B_{||}$ at $T = 0.25$ K. The best fit of Eq. (1) away from the avoided crossings gives $g_{\rm ens}/2\pi = 3.9$ MHz. Arrows point to satellites resulting from the hyperfine coupling of the electron spin to the nuclear spin of 13C atoms adjacent to some $P1$ centers (see Ref. [23] for further discussion). (c) Best fit $g_{\rm ens}$ to the $\lambda/4$ (circles) and $3\lambda/4$ (squares) modes as a function of temperature. Solid curves are the best fits of Eq. (2). Error bars are smaller than the symbol size.

and γ is the transition linewidth (assumed independent of m_I). As shown in Figs. 3(a) and 3(b), fitting the double-dip spectrum for the $3\lambda/4$ mode and the quality factors (Q) for $\lambda/4$ mode at 0.25 K using Eq. (1) yields collective coupling strengths $g_{\rm ens}/2\pi = 17.0 \pm 0.4$ and 3.9 ± 0.2 MHz, respectively, [23].

To investigate the temperature dependence of the collective coupling strength to each mode, we measure transmission spectra at several temperatures in the range 0.25–1.2 K and perform the same analysis as above [14,15,25]. The results are shown in Fig. 3(c) together with the best fits to

$$g_{\rm ens}(T) = g_{\rm ens}(0)\sqrt{P(B_\parallel, T)}, \qquad (2)$$

where $g_{\rm ens}(0)$ is the zero-temperature coupling strength, $P(B_\parallel, T) = \tanh(m_0 B_\parallel / 2k_B T)$ the spin polarization in thermal equilibrium, and k_B the Boltzmann constant. Two factors combine to make $g_{\rm ens}(T)$ higher for the $3\lambda/4$ mode. First, P increases monotonically with the Zeeman energy $m_0 B_\parallel$. Second, the bare spin-coupling strength g increases as $\sqrt{\omega_c}$ owing to a larger vacuum magnetic field strength with increasing mode number and a constant effective mode volume (the fraction of the resonator mode volume [9] occupied by the diamond sample is the same for both modes). The ratio 2.7 between the best-fit $g_{\rm ens}(0)/2\pi$ values for the $3\lambda/4$ and $\lambda/4$ modes (22.7 ± 0.6 and 8.3 ± 0.2 MHz, respectively) differs from the expected $\sqrt{3}$. This discrepancy may be due to inhomogeneous distribution of $P1$ centers in the mode volume [26] (see further below).

Having characterized coherent coupling in the hybrid system, we now turn to using the resonator as a probe of spin dynamics and equilibration. We first measure linewidth γ of the $m_I = +1$ transition in the dispersive regime [8], with ~ 70 MHz $\gg g_{\rm ens}/2\pi$ detuning between the $\lambda/4$ mode and $m_I = +1$ transition. We extract γ by inferring [23] the frequency shift (Δf) of the $\lambda/4$ mode immediately following a pump pulse whose frequency ω_p is stepped through the $m_I = +1$ resonance [Fig. 4(b)]. The pump pulse slightly decreases the polarization of the ensemble, redshifting the resonator. We fit a Lorentzian line shape to $|\Delta f|$, finding a full width at half maximum $\gamma/2\pi = 9.0 \pm 0.3$ MHz. A similar dispersive measurement using the $3\lambda/4$ mode at $B_\parallel = 263$ mT gives $\gamma/2\pi = 12.0 \pm 0.7$ MHz. We attribute the γ increase with $B_\parallel$ to the magnetic field inhomogeneity [23].

The spin relaxation time is measured by applying a pump pulse resonant with the $m_I = +1$ transition and monitoring the frequency shift in time as the spin polarization returns to equilibrium. We observe a biexponential decay response with time constants ~ 20 and ~ 160 s [Fig. 4(d)]. These constants are independent of temperature in the range 0.25–1 K [Fig. 4(e)], suggesting that spin polarization dynamics are governed by spin diffusion

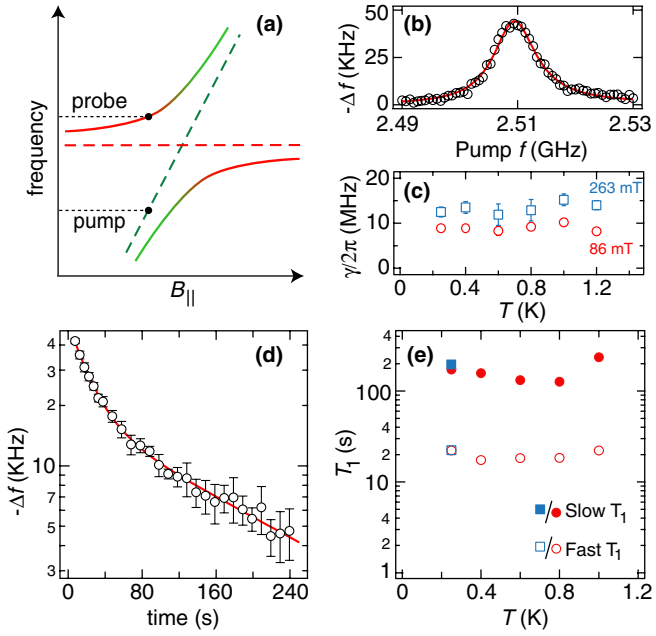

FIG. 4 (color online). Measurement of the spin linewidth and relaxation times using dispersive spin-resonator interactions. (a) Scheme (not to scale) for (b) the measurement of the spin linewidth ($T = 0.25$ K, $B_\parallel = 86$ mT) by probing the frequency shift of the $\lambda/4$ mode after applying a pump pulse (0.4s duration, -50 dBm incident power) through resonance with the $m_I = +1$ transition (60 s wait between successive measurements) [23]. A similar measurement of γ at $B_\parallel = 263$ mT is obtained using the $3\lambda/4$ mode. (c) γ at $B_\parallel = 86$ mT (circles) and $B_\parallel = 263$ mT (squares) as a function of temperature. (d) Measurement of the spin relaxation time T_1 by probing the resonator shift as a function of time after the pump pulse is switched off. A biexponential decay is observed. (e) Temperature dependence of the two time constants, extracted by probing with the $\lambda/4$ (circles) and $3\lambda/4$ (squares) modes. Error bars, unless shown, are smaller than the symbol size.

[20,27] rather than by spin-lattice relaxation [21]. Through dipolar flip-flop processes, the depolarization diffuses out of the resonator mode volume, leading to repolarization of the ensemble. The rate for this outdiffusion depends on the nominal dipolar coupling strength between spins in the ensemble, which itself depends on the spin density [12]. The two time constants may be explained by two diamond sectors inside the mode volume with electron-spin densities differing by a factor of ~ 8 [23,26,28]. Two observations lend further support to spin diffusion being the dominant spin relaxation mechanism: The relative amplitudes of the two exponentials do not change with temperature, and the two time constants remain unchanged upon varying the duration of the saturation pulses.

To investigate spin dynamics across subensembles, we measure how pumping one subensemble affects the polarization of other subensemble through cross relaxation [23]. As shown in Fig. 5(a), pumping at $f_{m_I=0}(B_\parallel)$ completely

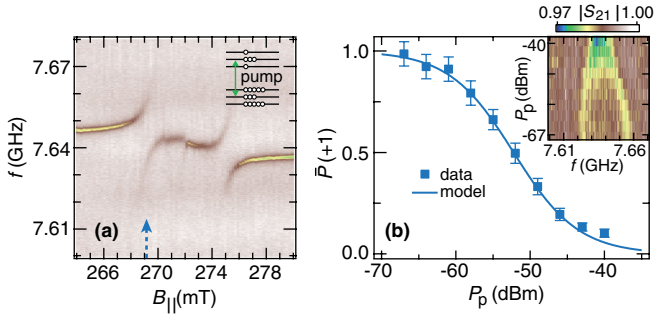

FIG. 5 (color online). (a) Transmission spectroscopy similar to Fig. 2(b), with an additional pump pulse resonant with the $m_I = 0$ transition (incident pump power $P_p = -50$ dBm, 100 ms duration) prior to $|S_{21}|$ measurement. Complete disappearance of the $m_I = 0$ avoided crossing and reduction in the coupling strength of the undriven transitions are observed. Color scale identical to Fig. 2(b). (b) Inset: Vacuum-Rabi-split dips at $B_\parallel = 269.1$ mT and pump frequency of 7.54 GHz as a function of P_p. The merging of dips with increasing P_p indicates cross relaxation between the subensembles. Main panel: Extracted polarization $\bar{P}$ (normalized to the value without pump) for the undriven $m_I = +1$ subensemble. The curve corresponds to the steady-state solution of a rate equation modeling fast equilibration between the subensembles compared to T_1 (see text and Ref. [23] for details).

suppresses the avoided crossing between the $m_I = 0$ transition and the resonator [29]. Remarkably, depolarization also occurs for the $m_I = \pm 1$ subensembles when pumping the $m_I = 0$ transition. The coupling strengths of the undriven transitions ($m_I = \pm 1$) to the $3\lambda/4$ mode are reduced to $g_{\mathrm{ens}}/2\pi = 12.5 \pm 0.5$ and 12.0 ± 0.5 MHz, respectively. To rule out the heating for the cause of depolarization, we pump off resonantly and observe no change of g_{ens} of the driven and undriven transitions. To quantify this steady-state cross relaxation, we measure the minimum splitting between the hybridized dips at $B_\parallel = 269.1$ mT [arrow in Fig. 5(a)] and pump frequency of 7.54 GHz as a function of pump power P_p. As shown in the inset of Fig. 5(b), the undriven $m_I = +1$ subensemble depolarizes further with increasing P_p. We can reproduce [23] this power-dependent steady-state cross depolarization using a rate equation including a spin diffusion rate Γ_o across the mode volume and a cross-relaxation rate Γ between subensembles [20]. We assume $\Gamma \gg \Gamma_o$ consistent with previous measurements of cross relaxation in high density $P1$-center samples by Sorokin *et al.* [28]. Under these assumptions, the steady-state normalized polarization of each subensemble is $\bar{P} = \Gamma_o/(\Gamma_o + \Omega_0/3)$, where Ω_0 is the pumping rate for the $m_I = 0$ transition. Excellent agreement is found with the model, with only the lever arm between Ω_0 and P_p as the free parameter. Using the best-fit lever arm in combination with Fermi's golden rule $\Omega_0 = 2\pi g^2 N_{\mathrm{phot}}/\gamma$ and the measured $\Gamma_o \approx 0.05\ \mathrm{s}^{-1}$ and $\gamma/2\pi \approx 12$ MHz, we estimate $g/2\pi \sim 2.5$ Hz. Note that N_{phot} is lower than on mode resonance by the filter factor $(\kappa_i + \kappa_e)^2/(\omega_c - \omega_p)^2$. Comparing this g to $g_{\mathrm{ens}}(T = 0)$ suggests $N \sim 10^{14}$ spins in the resonator mode volume.

In conclusion, we have used resonant and dispersive interactions with the two lowest-frequency modes of a NbTiN coplanar-waveguide resonator to probe the dynamics of a $P1$ electron-spin ensemble in diamond at low temperature and polarizing magnetic field. The observed temperature independence of spin relaxation time in the range 0.25–1 K supports spin outdiffusion as the dominant relaxation mechanism within the resonator mode volume. Resonant pumping of spin subensembles indicates exchange of Zeeman energies driven by dipolar interactions between the subensembles [20]. Follow-up experiments will pursue two directions: probing subensemble response to one or more resonant pump pulses on millisecond time scales to shed light on the cross-relaxation mechanism and cooling to 15 mK to fully polarize the ensemble [17] and extend spin coherence using subensemble-selective dynamical decoupling [18]. Ultimately, cross relaxation and achieved coherence will set the time scale over which subensembles may serve as independent quantum memories.

V. Ranjan and G. de Lange contributed equally to this work. We thank D. Ristè for experimental assistance and D. I. Schuster for helpful comments on the manuscript. We acknowledge funding from the Dutch Organization for Fundamental Research on Matter (FOM), the Netherlands Organization for Scientific Research (NWO, VIDI scheme), and a Marie Curie Career Integration Grant (L. D. C.).

[1] J. H. Wesenberg, A. Ardavan, G. A. D. Briggs, J. J. L. Morton, R. J. Schoelkopf, D. I. Schuster, and K. Mølmer, Phys. Rev. Lett. **103**, 070502 (2009).
[2] D. Marcos, M. Wubs, J. M. Taylor, R. Aguado, M. D. Lukin, and A. S. Sørensen, Phys. Rev. Lett. **105**, 210501 (2010).
[3] X. Zhu *et al.*, Nature (London) **478**, 221 (2011).
[4] Y. Kubo *et al.*, Phys. Rev. Lett. **107**, 220501 (2011).
[5] H. Malissa, D. I. Schuster, A. Tyryshkin, A. Houck, and S. Lyon, arXiv:1202.6305.
[6] Y. Kubo *et al.*, Phys. Rev. B **86**, 064514 (2012).
[7] A. Imamoglu, Phys. Rev. Lett. **102**, 083602 (2009).
[8] R. Amsüss *et al.*, Phys. Rev. Lett. **107**, 060502 (2011).
[9] Y. Kubo *et al.*, Phys. Rev. Lett. **105**, 140502 (2010).
[10] D. I. Schuster *et al.*, Phys. Rev. Lett. **105**, 140501 (2010).
[11] J. H. N. Loubser and J. A. van Wyk, Rep. Prog. Phys. **41**, 1201 (1978).
[12] J. A. van Wyk, E. C. Reynhardt, G. L. High, and I. Kiflawik, J. Phys. D **30**, 1790 (1997).
[13] M. V. G. Dutt, L. Childress, L. Jiang, E. Togan, J. Maze, F. Jelezko, A. S. Zibrov, P. R. Hemmer, and M. D. Lukin, Science **316**, 1312 (2007).

[14] P. Bushev, A. K. Feofanov, H. Rotzinger, I. Protopopov, J. H. Cole, C. M. Wilson, G. Fischer, A. Lukashenko, and A. V. Ustinov, Phys. Rev. B **84**, 060501 (2011).
[15] M. U. Staudt *et al.*, J. Phys. B **45**, 124019 (2012).
[16] J. Clarke and F. K. Wilhelm, Nature (London) **453**, 1031 (2008).
[17] S. Takahashi, R. Hanson, J. van Tol, M. S. Sherwin, and D. D. Awschalom, Phys. Rev. Lett. **101**, 047601 (2008).
[18] G. de Lange, T. van der Sar, M. Blok, Z.-H. Wang, V. Dobrovitski, and R. Hanson, Sci. Rep. **2**, 382 (2012).
[19] R. Barends, N. Vercruyssen, A. Endo, P. J. de Visser, T. Zijlstra, T. M. Klapwijk, P. Diener, S. J. C. Yates, and J. J. A. Baselmans, Appl. Phys. Lett. **97**, 023508 (2010).
[20] N. Bloembergen, S. Shapiro, I. S. Pershan, and J. O. Artman, Phys. Rev. **114**, 445 (1959).
[21] E. C. Reynhardt, G. L. High, and J. A. van Wyk, J. Chem. Phys. **109**, 8471 (1998).
[22] R. J. Cook and D. H. Whiffen, Proc. R. Soc. A **295**, 99 (1966).
[23] See Supplemental Material at http://link.aps.org/supplemental/10.1103/PhysRevLett.110.067004 for further description of the setup, measurement techniques, and data analysis.
[24] E. Abe, H. Wu, A. Ardavan, and J. J. L. Morton, Appl. Phys. Lett. **98**, 251108 (2011).
[25] K. Sandner, H. Ritsch, R. Amsüss, C. Koller, T. Nöbauer, S. Putz, J. Schmiedmayer, and J. Majer, Phys. Rev. A **85**, 053806 (2012).
[26] R. C. Burns, V. Cvetkovic, C. N. Dodge, D. J. F. Evans, M. L. T. Rooney, P. M. Spear, and C. M. Welbourn, J. Cryst. Growth **104**, 257 (1990).
[27] D. Suter and R. R. Ernst, Phys. Rev. B **32**, 5608 (1985).
[28] P. P. Sorokin, G. J. Lasher, and I. L. Gelles, Phys. Rev. **118**, 939 (1960).
[29] This is surprising from a single-spin perspective because the maximum Rabi driving strength ($f_{\mathrm{Rabi}} = g\sqrt{N_{\mathrm{phot}}}/2\pi \approx 100$ KHz for $N_{\mathrm{phot}} = 10^8$ photons on mode resonance) is significantly smaller than the spin linewidth.